LEGIBILITY NOTICE

A major purpose of the Technical Information Center is to provide the broadest dissemination possible of information contained in DOE's Research and Development Reports to business, industry, the academic community, and federal, state and local governments.

Although a small portion of this report is not reproducible, it is being made available to expedite the availability of information on the research discussed herein.

1

CONF-880724--1

LA-UR -87-4231

Los Alamos National Laboratory is operated by the University of California for the United States Department of Energy under contract W-7405-ENG-36

TITLE: MULTIPHASE FLOW IN THE ADVANCED FLUID DYNAMICS MODEL

AUTHOR(S): W. R. Bohl
D. Wilhelm
J. Berthier
F. P. Parker
S. Ichikawa
L. Goutagny
H. Ninokata
P. J. Maudlin

MASTER

DISCLAIMER

By acceptance of this article the publisher recognizes that the U S Government retains a nonexclusive royalty-free license to publish or reproduce the published form of this contribution or to allow others to do so for U S Government purposes

The Los Alamos National Laboratory requests that the publisher identify this article as work performed under the auspices of the U S Department of Energy

Los Alamos
Los Alamos National Laboratory
Los Alamos,New Mexico 87545

MULTIPHASE FLOW IN THE ADVANCED FLUID DYNAMICS MODEL

by

W. R. Bohl, D. Wilhelm, J. Berthier, F. P. Parker
S. Ichikawa, L. Goutagny, H. Ninokata, and P. J. Maudlin

ABSTRACT

This paper describes the modeling used in the Advanced Fluid Dy-
namics Model (AFDM), a computer code to investigate new approaches to
simulating severe accidents in fast reactors. The AFDM code has 12
topologies describing what material contacts are possible depending
on the presence or absence of a given material in a computational
cell, the dominant liquid, and the continuous phase. Single-phase,
bubbly, churn-turbulent, cellular, and dispersed flow are permitted
for the pool situations modeled. Interfacial areas between the con-
tinuous and discontinuous phases are convected to allow some tracking
of phenomenological histories. Interfacial areas also are modified
by models of nucleation, dynamic forces, turbulence, flashing, coa-
lescence, and mass transfer. Heat transfer generally is treated us-
ing engineering correlations. Liquid/vapor phase transitions are
handled with a nonequilibrium heat-transfer-limited model, whereas
melting and freezing processes are based on equilibrium considera-
tions. The Los Alamos SESAME equation of state (EOS) has been imple-
mented using densities and temperatures as the independent variables
A summary description of the AFDM numerical algorithm is provided.
The AFDM code currently is being debugged and checked out.
Two sample three-field calculations also are presented. The
first is a three-phase bubble column mixing experiment performed at
Argonne National Laboratory; the second is a liquid-liquid mixing ex-
periment performed at Kernforschungszentrum, Karlsruhe, that resulted
in rapid vapor production. We conclude that only qualitative compar-
isons currently are possible for complex multiphase situations. Many
further model developments can be pursued, but there are limits be-
cause of the lack of a comprehensive theory, the lack of detailed
multicomponent experimental data, and the difficulties in keeping the
resulting model complexities tractable

I. INTRODUCTION

The analysis of hypothetical core-disruptive accidents (HCDAs) in liquid-metal fast-breeder reactors (LMFBRs) is an inherently multiphase, multidimensional problem and involves many simplifying assumptions. At Los Alamos National Laboratory, an international team is working to develop approaches that will allow some approximations to be removed and the level of uncertainty to be reduced. These approaches are being implemented in a computer code called the Advanced Fluid Dynamics Model (AFDM). AFDM provides a prototype for testing developments leading to an improved HCDA computational capability. A previous paper[1] discussed the AFDM computational methods and gave the results of a preliminary calculation. This paper describes the models in AFDM and presents additional calculations, including a liquid-liquid-vapor system resulting in rapid vaporization.

In this paper, we first describe the scope of the AFDM code, including the differential equations and the components treated. Second, the overall AFDM algorithm is summarized. Third, we describe the AFDM models. This includes the treatment of topologies, flow regimes, interfacial areas, momentum-exchange and heat-transfer coefficients, and the solution to the intracell heat and mass-transfer equations. Finally, two sample calculations are presented showing the current status of the AFDM calculations. This allows some conclusions to be made and possible future developments to be discussed.

II. THE AFDM SCOPE

The AFDM may be categorized as a three-velocity-field, two-dimensional, multiphase, Eulerian, fluid-dynamics code. There are seven density components: structure, fuel particles, fuel liquid, coolant liquid, fuel vapor, coolant vapor, and noncondensable gas. The fuel particles and liquid occupy one velocity field, the liquid coolant occupies a second velocity field, and the vapor species are assigned to the third velocity field.

The differential equations involving mass, momentum, and internal energy that are solved in AFDM can be indicated schematically by

$$\frac{\partial \bar{\rho}_m}{\partial t} + \nabla \cdot (\rho_m \vec{v}_q) = \Gamma_m \quad, \tag{1}$$

$$\frac{\partial(\bar{\rho}_q \vec{v}_q)}{\partial t} + \nabla \cdot (\bar{\rho}_q \vec{v}_q \vec{v}_q) + \alpha_q \nabla p - \bar{\rho}_q \vec{g} + K_{qS} \vec{v}_q - \sum_{q'} K_{q'q} (\vec{v}_{q'} - \vec{v}_q)$$

$$- V\vec{M}_q = \sum_{q'} [\Gamma_{q'q} \vec{v}_{q'} - \Gamma_{qq'} \vec{v}_q] \quad . \tag{2}$$

$$\frac{\partial(\bar{\rho}_S e_S)}{\partial t} - Q_{KS} = Q_{HS} + Q_{NS} \quad , \tag{3}$$

$$\frac{\partial(\bar{\rho}_m e_m)}{\partial t} + \nabla \cdot (\bar{\rho}_m e_m \vec{v}_q) + p\left[\frac{\partial \alpha_m}{\partial t} + \nabla \cdot (\alpha_m \vec{v}_q)\right] - Q_{Km} = Q_{Hm}$$

$$+ Q_{\Gamma m} + Q_{Nm}. \quad \text{and} \tag{4}$$

$$\frac{\partial(\bar{\rho}_G e_G)}{\partial t} + \sum_{m=5}^{7} \nabla \cdot (\bar{\rho}_m e_m \vec{v}_G) + p\left[\frac{\partial \alpha_G}{\partial t} + \nabla \cdot (\alpha_G \vec{v}_G)\right] - Q_{KG} = Q_{HG}$$

$$+ Q_{\Gamma G} + Q_{NG} \quad . \tag{5}$$

The treatment of momentum by Eq. (2) includes a virtual mass term that provides a significant stability improvement, particularly when using higher order spatial differencing. The structure energy equation [Eq. (3)] has no mass-transfer source term, $Q_{\Gamma S}$, indicating that the structure volume fractions are independent of time. The mass transfers allowed are melting/freezing of particles and fuel liquid and the vaporization/condensation of both liquids with the respective vapor components. For consistency in mass and energy transport, the material components in the vapor energy equation [Eq. (5)] must be convected individually. Obtaining Eqs. (1)--(5) based on an averaging of local balance equations is still controversial. Additional terms to represent intercell momentum transfers, such as Reynolds stresses, currently are being considered.

In addition to Eqs. (1)--(5), AFDM attempts some following of phenomenological histories by convecting interfacial areas per unit mass using

$$\frac{\partial \bar{a}_q \bar{\rho}_q}{\partial t} + \nabla \cdot (\bar{a}_q \bar{\rho}_q \vec{v}_q) = \sum_A S_{A,q} + \sum_B S_{B,q} \quad . \tag{6}$$

In Eq. (6), the convectible interfacial areas each are assigned to a momentum field, and source (sink) terms exist for both the continuous liquid and the continuous vapor situations. Another possibility is to convect interfacial areas only with the velocity of the discontinuous phase, as is discussed in Sec. VIII.

III. THE AFDM ALGORITHM

The AFDM code integrates the differential equations on a staggered mesh with pressures, densities, energies, and interfacial areas defined on cell centers and velocities defined on cell edges. AFDM is designed to use a fractional-step method for time integration in which the intracell configuration changes and the heat/mass transfer are evaluated separately from intercell convection. This type of approach allows a modular development based on different viewpoints using differing theoretical formulations and increases the feasibility of expanding the equation set to treat the large number of components that may be considered in HCDA analysis.

There are four steps in the AFDM approach. Step 1 updates Eqs. (1)--(6) for intracell transfers. Convection is ignored, and the terms treated are the partial derivatives with respect to time (or the first term in each equation) and the mass and energy transfer terms (or the right side of each equation). The path through step 1 has eight parts as follows.

1. Evaluate the equation of state (EOS).
2. Select the flow topology and the continuous phase.
3. Update the convectible interfacial areas.
4. Define additional instantaneous interfacial areas for intracell transfers.
5. Obtain heat-transfer coefficients.
6. Calculate momentum-exchange coefficients.
7. Perform heat- and mass-transfer operations.
8. Modify convectible interfacial areas based on the mass-transfer results.

Step 2 initializes variables for the pressure iteration by integrating Eqs. (1)--(5) with the right sides set to zero and the convective terms treated explicitly. A van Leer[2] type of donor cell higher order spatial differencing is available as an option to reduce numerical diffusion. The virtual mass terms and the implicit treatment of interfield momentum coupling are described in Ref. 1. Interfacial areas are ignored because they are not included in the EOS. Step 3 obtains consistent end-of-time-step velocities and pressures using a multivariate Newton-Raphson iteration. A variation of the semi-implicit algorithm developed by Liles and Reed is used.[3] In the AFDM version of this approach, only selected (sensitive) variables or relationships are allowed to change from Step 2 estimates to limit the number of potential operations. Step 4 performs consistent convection of mass, momentum, energy, and interfacial area using the velocities from Step 3 to obtain the final end-of-time-step values for all the field variables. Because convection of interfacial area requires special considerations, it is discussed further in Sec. VIII.

One unique AFDM feature is the use of the SESAME[4] EOS package in a multi-phase code. The SESAME EOS system is a standardized, computer-based library of tables of thermodynamic properties and FORTRAN subroutines. To provide an interface for future adjustments with standard fast reactor safety EOS data,[5] the independent EOS variables are densities and temperatures. The materials are assumed to be immiscible; therefore, each component is evaluated with a separate EOS call. Volume fractions are determined using the principal of mechanical equilibrium; in other words, the particle and liquid components each must be compressed by an identical pressure. The difference between this EOS pressure and the cell pressure is one of the variables driving the step 3 iterative procedure. Another iteration requiring inversion of the EOS extracts temperatures as a function of internal energies following an update of the energy conservation equations. Saturation properties for the AFDM step 1 models are based on the vapor partial pressures. The AFDM models also require thermophysical properties (thermal conductivity, viscosity, and surface tension). These are computed outside of SESAME using separate correlations.

IV. INTERFACIAL AREA MODELING

A. Topologies

After an EOS call, the intracell transfer calculations in AFDM are started
by defining the geometric configuration of fluids in a computational cell,
called the topology. Once selected, the topologies are not changed during a
time step. The influence of the surrounding walls of the pool on the topology
selection is neglected. Therefore, we use the notation topology rather than
flow regime. Twelve topologies are generated to model the various combinations
of the three velocity fields. The physical parameters governing the choice are
the number of existing velocity fields, the dominant liquid within the two li-
quid velocity fields, and the dominant phase. Particles that form the solid
phase of velocity field one are assumed to possess a constant representative
radius. The subdivision into 12 topologies helps to set up an efficient logic
in the vectorized code. The topologies used by AFDM are shown in Fig. 1.

The dominant liquid is chosen as a function of the liquid and particle
volume fractions existing in a computational cell. The dominant or continuous
phase is determined by considering both volume fraction information and a levi-
tation criterion. The continuous phase is obvious for large vapor or liquid
volume fractions. The levitation criterion used for the intermediate case,
which evaluates whether liquid spheres of a size governed by a Weber number
can be levitated in a vapor flow driven by the local pressure gradient. If
so, vapor is the continuous phase. Hysteresis is assumed in order to avoid
numerical oscillations.

B. Flow Regimes

With the present set-up of topologies, some distinction among a limited
number of flow regimes already has been made. The droplet flow regime is de-
fined by choosing vapor as the continuous phase. Within liquid continuous
flows, we distinguish between four regimes: bubbly nucleating, bubbly, churn,
and cellular. The bubbly nucleating regime prevails for small bubble radii and
small vapor volume fractions and is characterized by bubbles being too small to
coalesce. Here, the nucleation model is used to update the interfacial areas.
(See IV.C.) Bubbly flow follows up to vapor volume fractions of about 0.3.

TOPOLOGY 1   TOPOLOGY 2   TOPOLOGY 3

TOPOLOGY 4   TOPOLOGY 5   TOPOLOGY 6

TOPOLOGY 7   TOPOLOGY 8   TOPOLOGY 9

TOPOLOGY 10   TOPOLOGY 11   TOPOLOGY 12

L1   liquid 1   G   vapor   S   structure
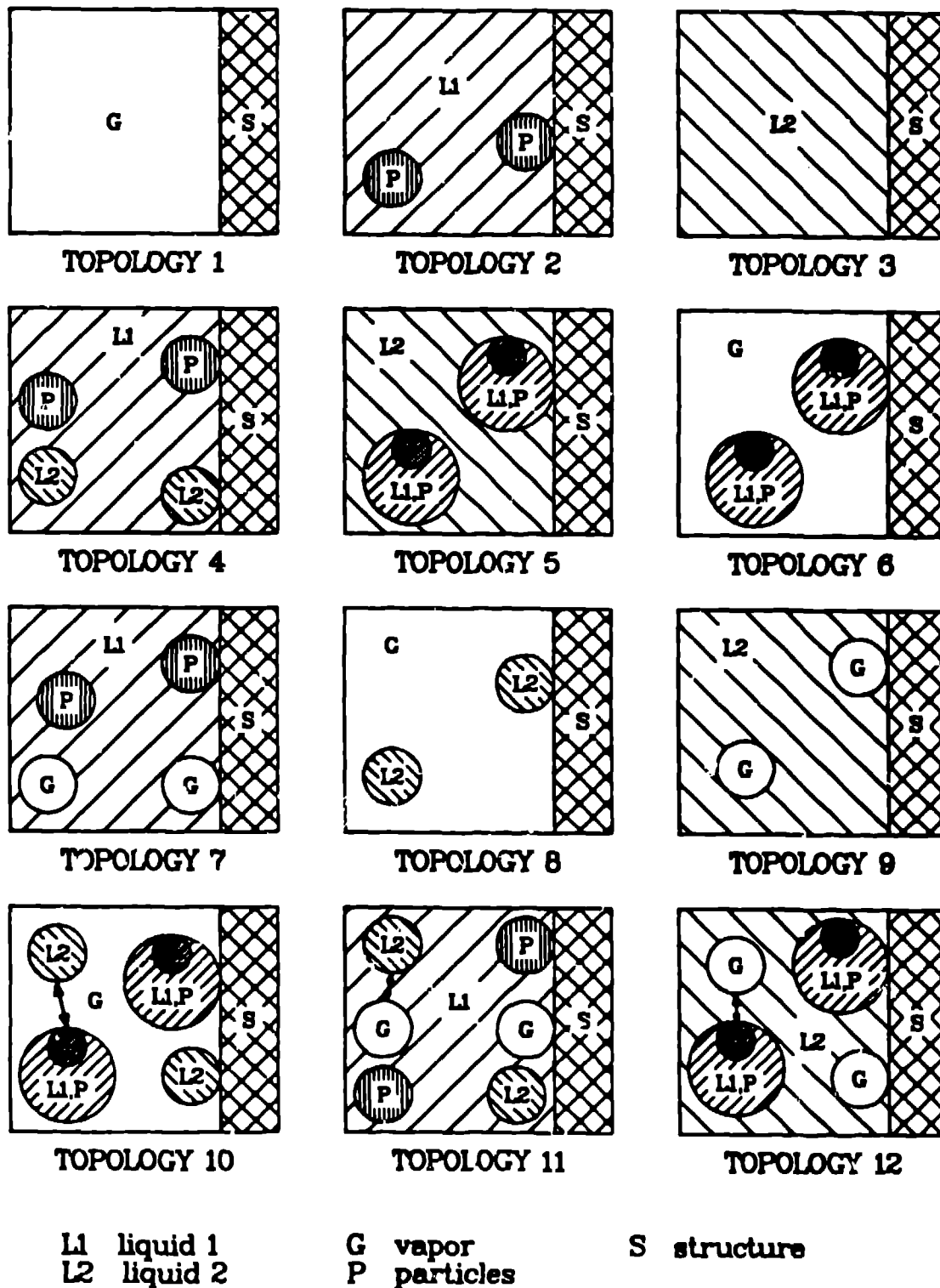L2   liquid 2   P   particles

Fig. 1.
The 12 topologies used by the AFDM computer code.

For higher void fractions, churn flow is indicated, which has an explicit effect on the calculation of the drag coefficient. (See Sec. VI.) All other effects with respect to surface areas and drag coefficients are taken care of implicitly by the use of a representative bubble size. For void fractions higher than about 0.5, a cellular flow regime is modeled when liquid continuous flow still prevails. Here, the liquid tends to form bridges between the bubbles, and the momentum exchange between the phases becomes large.

C. Calculations of Convectible Surface Areas

Bubbles and droplets form the discontinuous phases in the pool geometry. The models are restricted to evaluating spherical droplets or bubbles, which are called fluid spheres. However, the increase in surface areas beyond a spherical shape is taken into account by either multipliers or a model modification to describe the change of surface areas. Three surface areas are possible between the two discontinuous phases and the continuous phase, called here the convectible surface areas. Several source and sink terms exist that describe the splitting or coalescence of fluid spheres: nucleation, turbulence, dynamic forces, flashing, and random collision. We will discuss the source term resulting from dynamic forces as a representative example and will add limited information about the other processes.

To set up a model for the surface area source term, two physical quantities must be known. First, one needs to assess the equilibrium size of the fluid sphere under the conditions existing in the cell. Second, the rate with which equilibrium is achieved must be known. The equilibrium radius, r_e, can be described by a modified Weber criterion[6] with

$$r_e = \frac{We\sigma_{cd}}{4\rho_c \Delta v^2} + \left[\left(\frac{We\sigma_{cd}}{4\rho_c \Delta v^2} \right)^2 + C\frac{\mu_d^2}{\rho_d \rho_c \Delta v^2} \right]^{\frac{1}{2}} \quad , \tag{7}$$

where We is the Weber number, which may be different for bubbles and droplets, and where the indices c and d indicate continuous and discontinuous phases, respectively. The second term of the square root accounts for the effects of viscous flow fields with a constant, C, to be a user-defined input. A single-relaxation-time model is used with

$$\frac{d}{dt}r_d = \min\left(\frac{r_e - r_d}{\tau}, 0\right) ,$$ (8)

where the time constant, τ, is defined using[7]

$$\tau = \frac{C' r_d}{\Delta v}\left(\frac{\rho_d}{\rho_c}\right)^{\frac{1}{2}} .$$ (9)

with another user-defined constant, C'. Equation (8) is integrated over a time step, Δt, to yield the change in radius, Δr. The surface area, a, is a function of the radius and the volume fraction, the latter of which stays constant during this part of the update. The change in surface area, Δa, is now

$$\Delta a = 3\alpha_d\left(\frac{1}{r_d + \Delta r_d} - \frac{1}{r_d}\right) .$$ (10)

A turbulence break-up model is introduced for fluid spheres that exist in a continuous liquid phase.[8] The energy of the turbulence eddies is assumed to be proportional to the interphase velocity, and a gravity term provides a value at low velocities. Turbulence generated by bubbles can disrupt not only bubbles but also droplets of the discontinuous liquid. A flashing model is used only for the break-up of droplets in a continuous vapor phase. The internal overpressure of droplets at the bulk temperature is compared with the pressure that can be accommodated by surface tension. Random collision is taken into account with both liquid and vapor continuous phases. The rate of surface area change is proportional to the interphase velocity and the volume fraction of the dispersed phase.

Usually, the convectible surface areas are functions of the volume fractions and the sphere radii. However, to be able to describe the nucleation of bubbles in a continuous liquid, the surface areas in low-vapor-volume-fraction pools are functions of the number density of nucleating bubbles[9] and the volume fractions. The change in number density is a function of a dimensionless superheat to model delays in nucleation during rapid evaporation.

D. Determination of Instantaneous Interfacial Areas

After the convectible surface areas are updated, they must be subdivided in case a given topolcgy has more than one discontinuous component and/or structure. Step 1 calculates up to 10 instantaneous surface areas between the components given in a cell by introducing several models, as there is liquid 1-particle contact based on melting-freezing criteria, two-phase two-liquid contact at zero velocity difference based only on surface tension criteria, contact of two discontinuous components because of random collision at finite velocity difference, and a combination of the latter two processes. Additionally, weighting factors are introduced to redirect bubble surfaces to the liquid that undergoes nucleation.

For example, for two-phase two-liquid contact at zero velocity differences, a model becomes necessary because the two liquids may co-exist in a given cell. Based on surface tension observations,[10] three configurations are possible in AFDM as shown in Fig. 2. Here, c and d denote the continuous and discontinuous liquid, respectively, and g denotes the vapor phase. The model is not necessary for all continuous vapor topologies because droplet-droplet interaction is modeled by random collision. In Fig. 2, the three configurations depend on two surface tension parameters:

$$\sigma_1 = \sigma_{cg} - \sigma_{dg} - \sigma_{cd} \quad , \text{ and} \tag{11}$$

$$\sigma_2 = \sigma_{dg} - \sigma_{cg} - \sigma_{cd} \quad . \tag{12}$$

where the three surface tensions between vapor and continuous liquid, cg; vapor and discontinuous liquid, dg; and between both liquids, cd, must be known. For configurations 1 and 3, the observation predicts a very limited contact between the vapor bubble and one of the liquid phases. However, to restrict the exclusiveness of this observation, a user-defined residual surface area, a_r, is introduced.
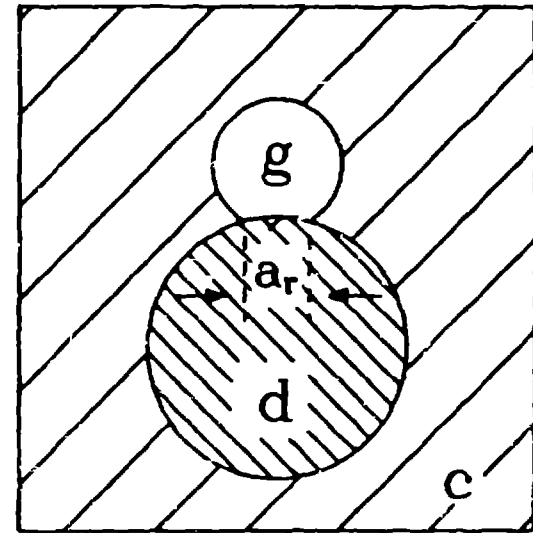
The increased contact between discontinuous vapor and discontinuous liquid spheres in case that film boiling criteria are met is taken into account only by changing the heat-transfer coefficients.
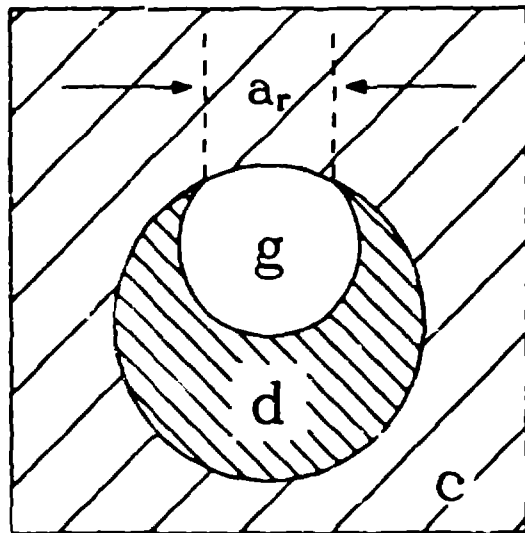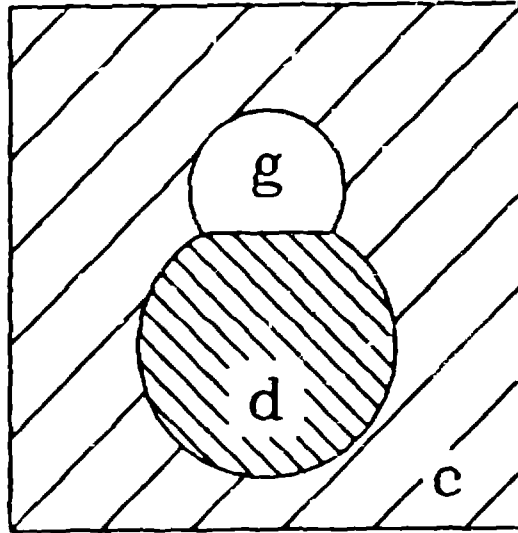
Configuration 1   Configuration 2   Configuration 3

c   Continuous liquid

d   Discontinuous liquid

g   Vapor bubble

Fig. 2.
Two-phase, two-liquid configurations in AFDM.

V. HEAT-TRANSFER COEFFICIENTS

After the instantaneous interfacial surface areas are evaluated, heat-transfer coefficients are calculated assuming steady-state temperature profiles. Between liquid, structure, and particle component pairs, heat transfer is based on bulk temperature differences. Heat transfer to or from the vapor field is based on interface temperatures. When mass transfer occurs, the interface temperature is the saturation temperature corresponding to the partial pressure of the participating component. If no mass transfer is possible, the interface temperature is evaluated to obtain heat flow continuity. A general expression of the heat flux for a nonvapor component, m, is

$$Q_{Hm} = \sum_{m'} h_{m,m'} a_{m,m'} (T_{m'} - T_m) + h_{m,G} a_{m,G} (T^I_{G,m} - T_m) \quad , \tag{13}$$

where m' $\neq$ m, and m' $\neq$ G. For the vapor,

$$Q_{HG} = \sum_m h_{G,m} a_{G,m} (T^I_{G,m} - T_G) \quad . \tag{14}$$

where m $\neq$ G. The heat-transfer processes considered are conduction, convection, and radiation. In general, a convective correlation of the Nusselt number is used in the continuous phase.[11] For the discontinuous phases, convective heat-transfer correlations are used if the droplet is in the nonrigid mode. For the rigid mode, a conductive heat-transfer coefficient is assumed. A special case is given for particles and continuous liquid 1 where additional turbulent heat transfer is taken into account. Both components are in the same velocity field, but they do not have the same turbulent velocity fluctuations. Another special case occurs between liquid droplets when the vapor is the continuous phase. Both liquid droplets exchange heat by direct contact during collision and by radiation. A third special case corresponds to film boiling. In case of the contact of two liquids, a stable film exists if the difference between the interface temperature and the liquid 2 saturation temperature is above the Leidenfrost point. The heat-transfer coefficient then is based on a combination of the convective and radiative Nusselt numbers inside the vapor

film.[12] Heat-transfer coefficients are calculated explicitly and are not changed during the heat- and mass-transfer calculations.

VI. CALCULATION OF MOMENTUM EXCHANGE COEFFICIENTS

The momentum exchange coefficients of Eq. (2) are functions of drag coefficients and instantaneous interfacial areas. They consist of a laminar and a turbulent term. The laminar term is only a function of the viscosity, but the other is directly proportional to the velocity difference between the velocity fields under consideration. The main parameter of the turbulent term is the drag coefficient, which, in case of the drag between the discontinuous and the continuous fields, is calculated using a drag similarity hypothesis.[13] Therefore, a model is implemented that uses fluid spheres similarly to the model for the surface area source and sink terms. For modest velocity differences, the model calculates a mixture viscosity using data from both the continuous and discontinuous phases. The Reynolds number of the fluid spheres is based on this viscosity. The influence of distortion of the spheres and of the volume fraction on the drag coefficient is accounted for by introducing terms that compare surface tension forces with gravity forces and those that are functions of the volume fractions.

For liquid continuous flows with high void fractions, the drag coefficient is compared with that of a churn-turbulent lower limit. For void fractions higher than about 50% but still prevailing continuous liquid flows, the drag coefficient is assumed to increase substantially because this flow regime exists only for low vapor slip velocities.

Generally, momentum exchange coefficients between two discontinuous components or a discontinuous component and the structure do not imply a laminar term, and constant drag coefficients are assumed. However, if film boiling is indicated, the momentum exchange coefficient between the vapor and the discontinuous liquid is increased to model at least a part of the vapor phase existing as a blanket around the liquid spheres

VII. INTRACELL UPDATES FOR HEAT AND MASS TRANSFER

A. Introduction

With the interfacial areas and heat-transfer coefficients known, the truncated AFDM Step 1 conservation equations are solved. The mass-transfer determination is nonlinear and has received the most attention. A three-step

process is involved. First, vaporization-condensation is determined. Second, melting and/or freezing rates are evaluated. Third, velocities and convective interfacial areas are updated based on mass-transfer results.

B. Vaporization and Condensation

Two different models are used, depending on the presence or absence of vapor in a cell. For a two-phase cell, interfaces exist between liquid and vapor, and a total heat flux balance can be calculated at the interfaces. In the present code, mass transfer is only driven thermally, and there are no limitations because of diffusion processes. Mass-transfer rates are determined by summing Eqs. (3)--(5) and then using the fact that overall energy conservation can be maintained if all the heat- and mass-transfer sources are summed to zero for each material (including both liquid and vapor components). This gives a mass-transfer rate of the form

$$\Gamma_{G,Lm} = \frac{Q_{HS,m} + Q_{HP,m} + Q_{HL,m} + Q_{HG,m}}{H(\Gamma_{G,Lm})(i_{Gm} - i_{Con,m}) + H(-\Gamma_{G,Lm})(i_{Vap,m} - i_{Lm})} \quad . \tag{15}$$

In Eq. (15), the difference between the interfacial enthalpy and the bulk enthalpy must be included in the effective heat of vaporization because the only permanent energy variable stored is the bulk value. The mass-transfer rate then is back-substituted into the energy conservation equations. The equations are solved by identifying two types of variables, sensitive and insensitive. The sensitive variables are T_{L1}, T_{L2}, T_G, $\bar{\rho}_{L1}$, and $\bar{\rho}_{L2}$, the less sensitive variables are T_S and T_P. The sensitive variables are updated implicitly with a multivariate Newton-Raphson procedure. The less sensitive variables are updated explicitly with limiters on the heat-transfer coefficients to avoid overshoots. The main difficulty with this procedure is the apparent tendency of the Jacobian matrix in the Newton-Raphson iteration to become singular when the products of the heat-transfer coefficients times the interfacial areas are much larger than the liquid thermal inertia. At these points, which component vaporizes and which component condenses apparently becomes indeterminate. Solutions to this problem are being studied.

The method is different for a single-phase cell where no interfacial heat flux can be calculated. In such a case, heat transfer between the two liquid components, the particle field, and the structure is calculated implicitly by

solving a 4 x 4 system of linear equations. Mass transfer then is required only to initialize a fictitious vapor volume used for numerical convenience. This is determined by using the departure from saturation conditions resulting from the heat-transfer calculation as a driving source in the energy conservation equations.

C. Melting and Freezing

The rate of melting/freezing is obtained by an equilibrium model. The energies of the liquids and particles come from the calculations in Sec. VII.B. The freezing rate is proportional to the difference between the liquidus energy and the energy of liquid 1. The melting rate is proportional to the difference between the particle energy and the solidus energy of component 1. The residual liquid (in freezing) or residual particles (in melting) remain at the liquidus or solidus energies, respectively. If all of a component can freeze or melt, a direct energy-field transfer occurs to ensure energy conservation.

D. Update of Velocities and Interfacial Areas

When the Γ_{qq}' are available, the velocities can be updated consistently with the energies and densities using Eq. (2). Also, using the mass-transfer rates, data are available to update the convectible interfacial areas a second time. All surfaces areas are functions of the volume fractions. Therefore, the change in volume fractions must be taken into account in the area updates. If new volume fractions are generated by phase transitions, initial surface areas and initial momentum coupling coefficients are associated with them.

VIII. INTERFACIAL AREA CONVECTION

Discussion of the details of Steps 2--4 of the AFDM algorithm is beyond the scope of this paper. (See Ref. 1.) However, the convection of interfacial areas in Step 4 deserves additional comment. Two methods of interfacial area convection have been programmed in AFDM: the currently operational method follows Eq. (6). Each interfacial area is assigned to a momentum component. The area per unit volume is divided by the appropriate density component, and then the area per unit mass is convected similarly to the specific internal energy with higher order differencing (if specified). Consequently, this approach

convects interfacial area for both the continuous and the discontinuous components. The second, exploratory, approach is to only convect interfacial area using the velocity of the discontinuous phase. The idea is to better treat the change in topology that can occur at a cell interface. Here interfacial area is not associated with a unit of mass or volume, and consistent higher order differencing appears impossible. As an example, consider area being convected from a cell with bubbly flow to one with droplet (dispersed) flow. The current approach would move the interfacial area with the liquid such that the droplet source in the dispersed cell would correspond to the bubble size in the liquid continuous cell. The exploratory approach would move the interfacial area with the vapor velocity so that the droplet source likely would be larger or smaller than the bubble size in the donor cell. The questions raised by such considerations require significant further study.

IX. SAMPLE CALCULATIONS

Currently, the AFDM code is being debugged and checked out, and the results of both simple and more complex problems are being studied. This paper presents one problem of each type.

A. A Three-Phase Bubble Column Simulation

The "simple" problem was a study by Argonne National Laboratory[14] of the onset of mixing and stratification within liquid-liquid and liquid-solid mixtures agitated by gas bubbling. The experimental data led to the hypothesis that separation (or mixing) is determined in quasi-static situations by comparing the mean density of the mixture, $\bar{\rho}_{Mix} = \Sigma \bar{\rho}_m$, with the density of the lighter component, $\rho_{\ell x}$. Starting from a stratified configuration, initial mixing will begin when $\rho_{\ell x} > \bar{\rho}_{Mix} = \rho_{hx}\alpha_{hx}$. Stratification from a mixed configuration occurs when $\rho_{\ell x} < \bar{\rho}_{Mix} = \rho_{\ell x}\alpha_{\ell x} + \rho_{hx}\alpha_{hx}$.

The AFDM code can reproduce such behavior qualitatively simply by using the hypothesis that only the largest volume-fraction liquid has liquid/vapor momentum coupling in liquid continuous flow. For example, the quasi-static pressure gradient is $\nabla p = \bar{\rho}_{Mix} q$. If $\rho_{hx}\alpha_{hx} < \rho_{\ell x}$ in the lower fluid of a stratified situation, a small amount of numerical mixing will progressively allow downflow of the lighter fluid into the heavier fluid as a consequence of the AFDM momentum equations.

Several AFDM calculations have been run to examine this situation. Figure 3 shows the results when the lighter fluid has a specific gravity of 0.87 (p-xylene), the heavy fluid is water, and the gas flow has been set to zero to achieve a optimal stratification rate.

B. A Liquid-Liquid Mixing Experiment with Vapor Production

One of the early tests of Step 1 performance was done on the small-scale multicomponent multiphase box (MMB) experiment currently under way at Kernforschungszentrum, Karlsruhe (KfK). The experiment was chosen because it incorporates many features that address AFDM Step 1 modelling. The experimental hardware consists of a rectangular 10-cm x 21-cm x 3-cm box partially made of glass walls to permit observation with a high-speed movie camera. Figure 4 shows a front view of the box. Because the center line is a symmetry axis, the left side shows a simplified initial state of the experiment, whereas the right side shows the code model in a quasi-planar geometry. We have added cell numbers to Fig. 4. A cell is identified by reading the horizontal and the vertical number in that order. The box is cooled to 240 K and filled with liquid ammonia. A hollow cylinder 2.5 mm thick separates the ammonia from a voided center region that is filled with hot tetralin (a hydrocarbon immiscible with ammonia) shortly before the test.

The experiment is initiated by withdrawing the separating cylinder into the back wall of the box. The movement of the cylinder is completed after about 100 ms, and it introduces turbulence at the liquid-liquid interface. This part of the transient is difficult to model with the code, and adjustments for the starting time become necessary, as mentioned below. The experiment is designed to simulate the hydrodynamic interaction of two immiscible liquids with differing densities. The initial temperature of tetralin is above the saturation temperature of ammonia. As ammonia evaporates, the liquid-liquid mixing process is enhanced. The droplets of the discontinuous liquid are split up, increasing the interfacial surface area between the liquids. Finally, a vigorous evaporation of ammonia takes place after several hundred milliseconds, leading to a complete mixing and thermal equilibration of the liquids. The final stage is governed by the stratification of the nonevaporated ammonia above the tetralin.

The initial conditions of the AFDM calculation, as given by the experiment, are as follows.

- Initial temperature of liquid ammonia: 225 K (The saturation temperature at 1 bar is 240 K.)
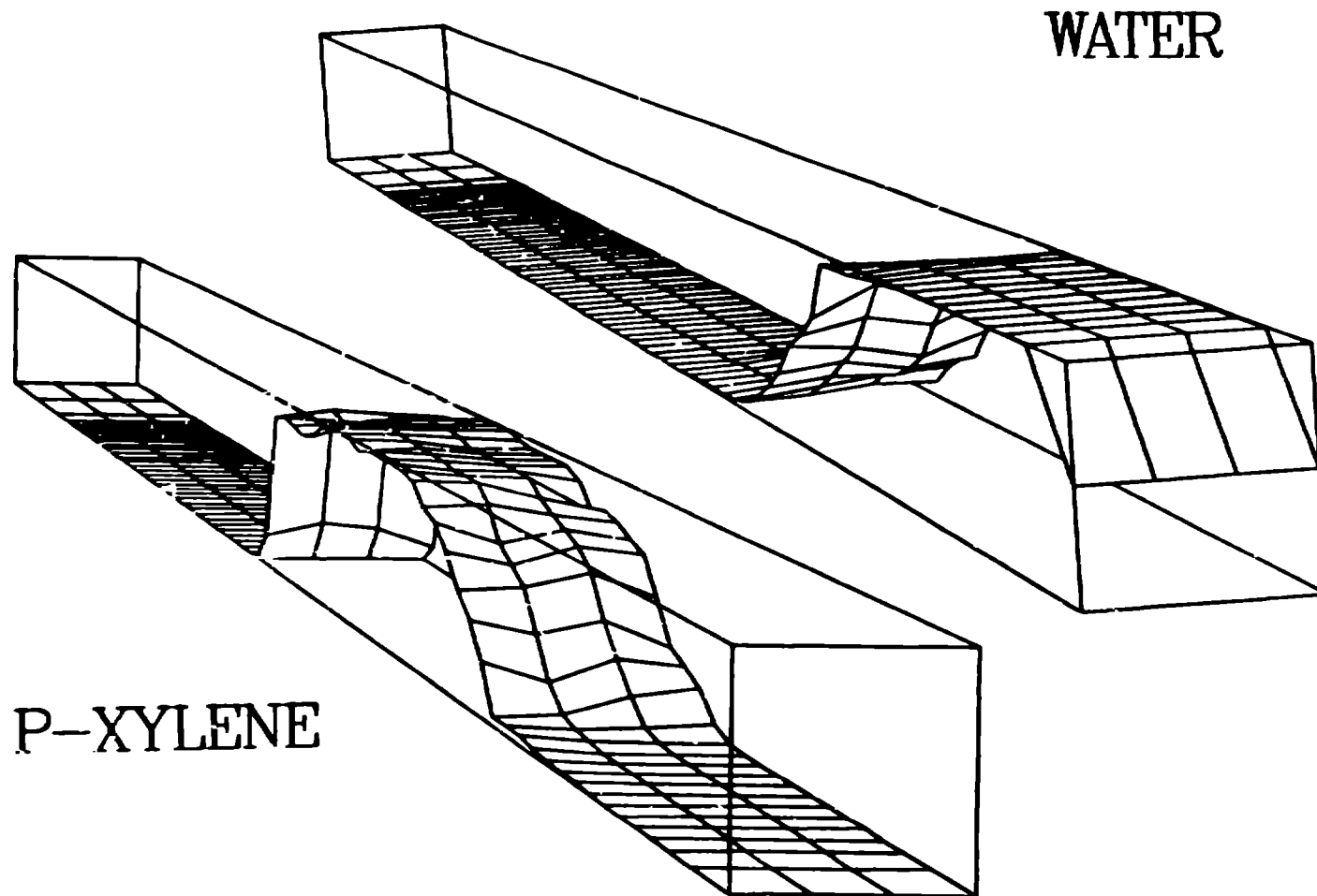
WATER

P-XYLENE

Fig. 3.

An AFDM calcuiation in the process of stratification. Shown are the liquid volume fractions in a bubble column of radius 35 mm and height 1 m. The lower boundary node is 50% structure volume to channel gas flow upward.
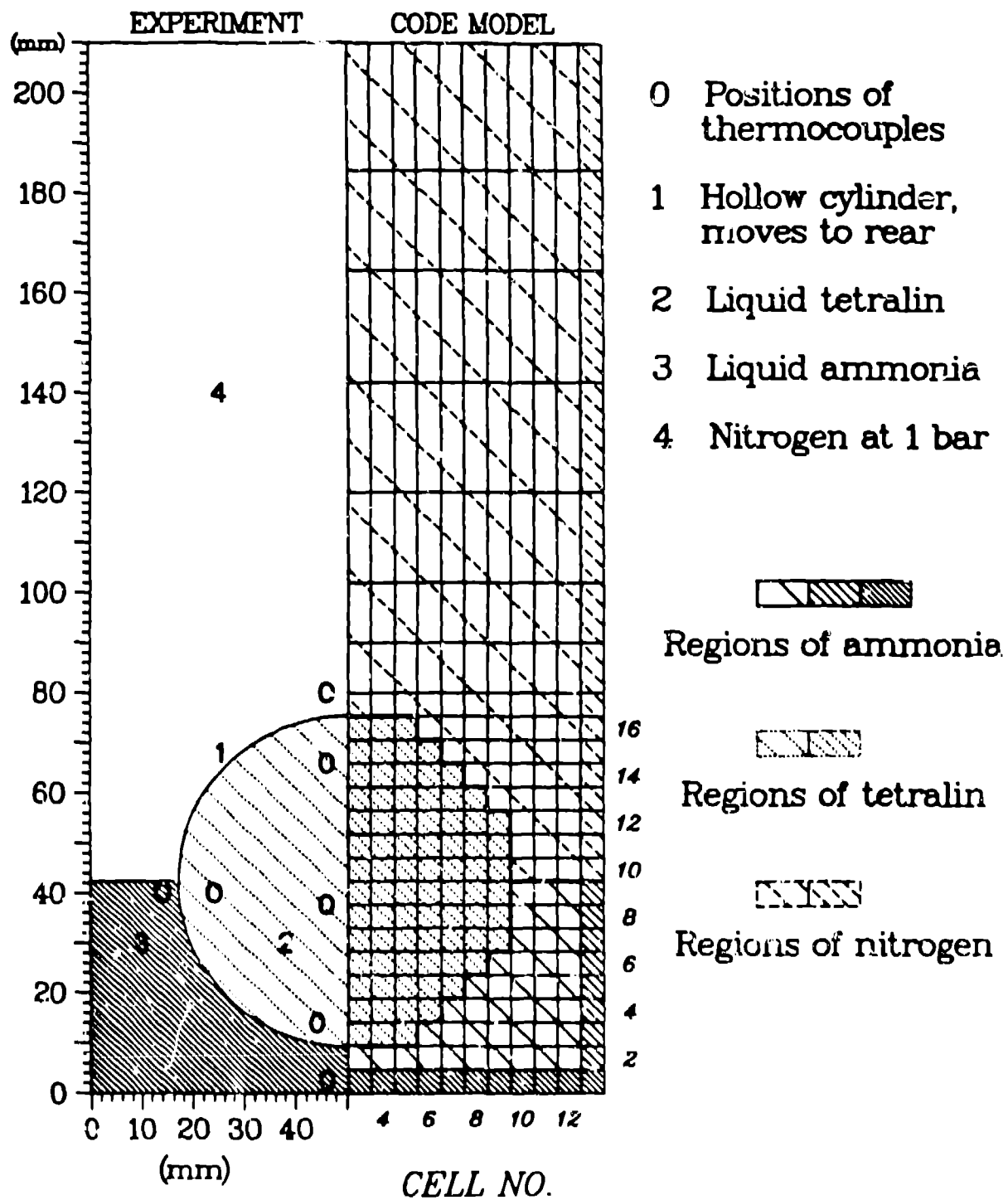
Fig. 4.
Experimental/calculative setup for the KfK MMB experiment.

- Initial temperature of liquid tetralin: 319 K (The saturation temperature at 1 bar is 350 K.)
- Ammonia mass: 0.039 kg. Tetralin mass: 0.104 kg density ratio ammonia/tetralin: 0.7.

At this stage of the code shake-down program, no substantial effort could be expended to examine the effects of modifications on about 70 parameters available to tune the Step 1 models. However, the code was able to address the main physical phenomena occurring during the transient. A selection of results is given below.

As in the experiment, the AFDM calculation can be divided into three parts. First, premixing takes place as the heavier tetralin moves down through the liquid ammonia. In the contact region between the liquids, vapor is generated, which enhances the mixing process. Figure 5 shows the convectible interfacial areas for the cell [(7,4)] that represents the lower mixing region. Between 0 and 150 ms, the surface area stays at a low value of about 10 m^2/m^3. As slip velocities increase, so does the interfacial area, which results in a rapid change just before 200 ms. At this time, the rapid evaporation leads to a pressure pulse, which is shown in Fig. 6. In this second stage, the pressure drives both liquids upward. The large velocities generated are responsible for a rapid redistribution of the masses, and the liquids now fill a much larger volume. Droplet flow with topology 10 is dominant. The splitting processes now yield surface areas on the order of 10 000 m^2/m^3. The calculated pressure pulse of Fig. 6 is observed in the experiment at 400 ms.

As stated above, the experimental starting time needs adjustment. If the starting time is postponed by 200 ms, the pressure pulses of both the code and the experiment occur at the same time. Using the same time shift, a comparison of tetralin temperatures in cell (8,9) with experimental temperatures is shown in Fig. 7. Because the position of this cell is near the periphery of the initial tetralin region, the initial change in temperature is sensitive to how the interface between both liquids moves. The third stage of the transient is characterized by sloshing of the liquids and, finally, a stratification of the liquid ammonia above the tetralin. Figure 7 shows that both experiment and code predict hot tetralin reentering cell (8,9) between 600 and 500 ms. The final stage of stratification is not shown in Figs. 5--7 because it takes more than 2000 ms. However, the comparison with the experiment is reasonable.
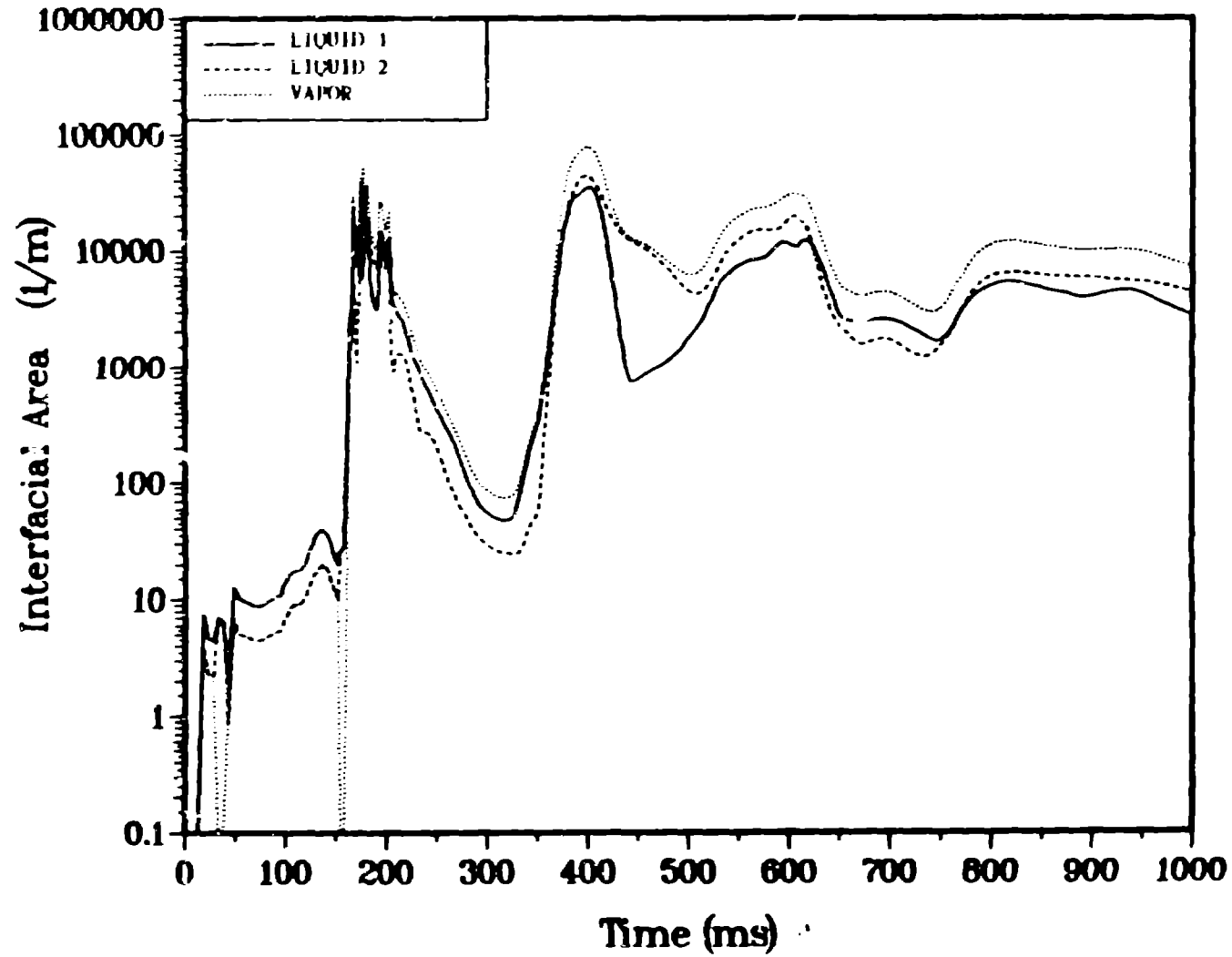
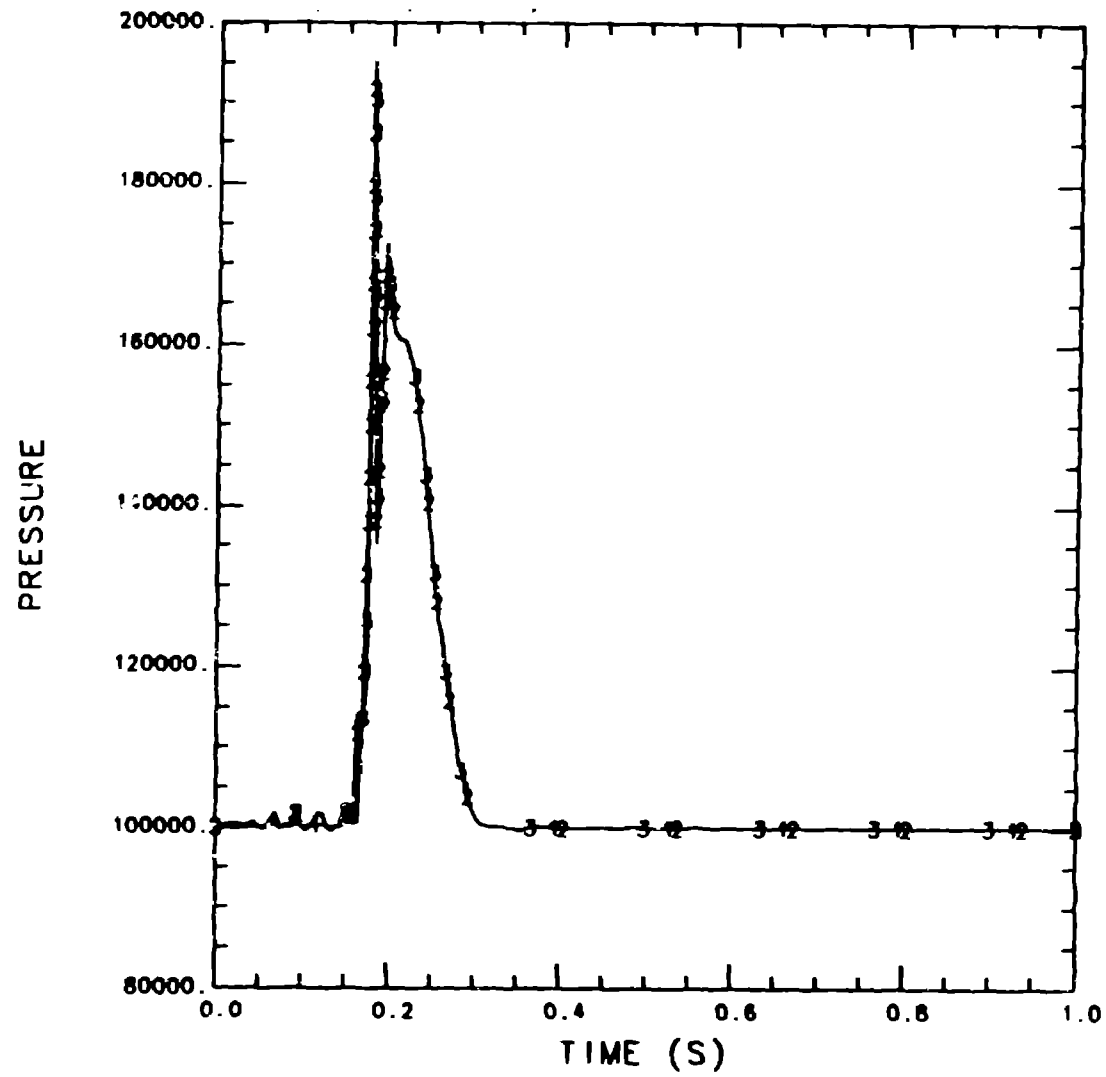# MMB-119 EXPERIMENT CELL (7,4)

Fig. 5.
Calculated convectible surface area in the lower mixing region.

MINIMUM VALUE= 9.95223E+04
MAXIMUM VALUE= 1.95098E+05

Fig. 6.
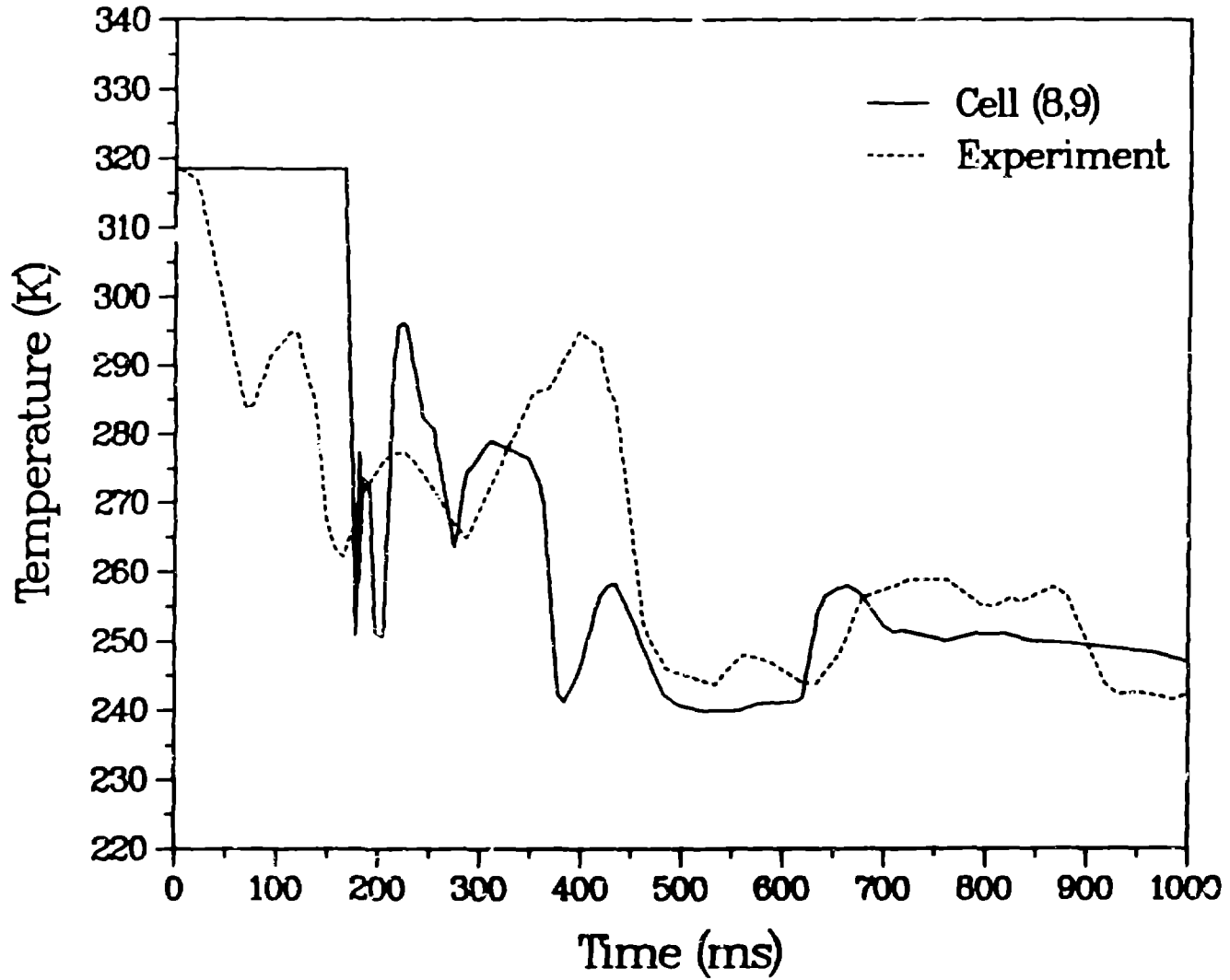Calculated pressures in the MMB experiment.

Fig. 7.
Calculated temperatures compared with thermocouple readings in the MMB experiment.

The higher order differencing scheme was found to be important. Using simple donor-cell differencing, the Step 1 AFDM models were dominated by diffusion. The main "simple" model modification suggested by this experiment is replacement of the bulk liquid-liquid heat-transfer term in Eq. (13) by a term that only transfers heat between the surfaces of the two liquids with the appropriate modifications to the mass-transfer models, which would better represent the film boiling regime. Advanced modifications, such as better representing experimental turbulence, would take considerably more effort.

X. CONCLUSIONS

The AFDM code brings a new level of sophistication into modeling the details of multicomponent, multiphase flow, and the modelling shows promise. Relatively simple models, combined with a detailed solution to the conservation equations, evidently can represent the dominant features of multiphase flow. In particular, the calculations presented here suggest an application of AFDM, with some simple model modificatons, in future investigations of vapor explosions. Examining the effects of the various model parameters also should be profitable.

Many extensive improvements can be suggested. Besides turbulence, channel flow regimes require representation, more components could be added for transport of distorted droplet/bubble shapes or temperature gradients, and mass transport could be modelled in a more integrated, nonequilibrium, diffusion-limited fashion. Unfortunately, the extensive numerical complexity, the lack of a complete theory, and the limited detailed experimental data base do pose limits. Further development can make progress in addressing LMFBR HCDA issues, but perhaps the best question to address in future efforts is the optimal development strategy given the resources available to the project.

REFERENCES

1. W. R. Bohl, D. Wilhelm, F. R. Parker, J. Berthier, P. J. Maudlin,
    P. Schmuck, L. Gutagny, S. Ichikawa, H. Ninokata, and L. B. Luck,
    "Computational Methods of the Advanced Fluids Dynamics Model," in Proc. of
    the International Topical Meeting on Advances in Reactor Physics,
    Mathematics, and Computation (American Nuclear Society, La Grange Park,
    Illinois, 1987), pp. 1625-1640.

2. B. van Leer, "Towards the Ultimate Conservative Difference Scheme. IV.A
    New Approach to Numerical Convection," J. Comp. Phys. 23, 276-299 (1977).

3. D. R. Liles and W. H. Reed, "A Semi-Implicit Method for Two-Phase Fluid Dynamics," J. Comp. Phys. $\underline{26}$, 390-407 (1978).

4. B. I. Bennett, J. D. Johnson, G. I. Kerley, and G. T. Rood, "Recent Developments in the Sesame Equation-of-State Library," Los Alamos Scientific Laboratory report LA-7130 (February 1978).

5. J. K. Fink, M. G. Chasanov, and L. Leibowitz, "Properties for Reactor Safety Analysis," Argonne National Laboratory report ANL-CEN-RSD-82-2 (May 1982).

6. G. Kocamustafaogullari, I. Y. Chen, and M. Ishii, "Unified Theory for Predicting Maximum Fluid Particle Size for Drops and Bubbles," Argonne National Laboratory report ANL-84-67, NUREG/CR-4028 (1984).

7. S. A. Krzeczkowski, "Measurement of Liquid Droplet Disintegration Mechanism," Int. J Multiphase Flow $\underline{6}$. 227-239 (1980).

8. M. Sevik and S. H. Park, "The Splitting of Drops and Bubbles by Turbulent Fluid Flow," J. Fluid Engng. $\underline{95}$, 53-60 (1973).

9. N. Abuaf, B. J. C. Wu, G. A. Zimmer, and P. Saha, "A Study of Nonequilibrium Flashing of Water in a Converging-Diverging Nozzle," Brookhaven National Laboratory report BNL-NUREG-51317, NUREG/CR-1864 (1984). Vol. 2.

10. Y. H. Mori, "Configuration of Gas-Liquid Two-Phase Bubbles in Immiscible Liquid Media," Int. J. Multiphase Flow $\underline{4}$, 383-396 (1978).

11. S. Sideman, "Direct Contact Heat Transfer Between Immiscible Liquids," in Advances in Chemical Engineering (Academic Press, New York, 1966).

12. F. S. Gunnerson and A. W. Cronenberg, "Film Boiling and Vapor Explosion Phenomena," Nuclear Technology $\underline{49}$, 380-391 (1980).

13. M. Ishii and N. Zuber, "Drag Coefficient and Relative Velocity in Bubbly, Droplet, or Particulate Flows," AIChE Journal $\underline{25}$(5) 843-855 (1979).

14. M. Epstein, D. J. Petrie, J. H. Linehan, G. A. Lambert, and D. H. Cho, "Incipient Stratification and Mixing in Aerated Liquid-Liquid or Liquid-Solid Mixtures," Chem. Engng. Sci. $\underline{36}$(4), 784-787 (1981).

NOMENCLATURE

a	Interfacial area per unit volume
$\bar{a}$	Interfacial area per unit mass
C	User-defined constant
C'	User-defined constant
e	Specific internal energy
$\bar{g}$	Acceleration from gravity
h	Heat-transfer coefficient
H	Heaviside function
i	Enthalpy
K	Interfield momentum exchange coefficient
p	Pressure
Q	Volumetric energy source term
r	Radius
S	Interfacial area source term
t	Time
T	Temperature
$\dot{v}$	Velocity
$\overrightarrow{VM}$	Virtual mass term
We	Weber number
α	Volume fraction
Γ	Mass-transfer rate per unit volume
Δv	Interfacial slip velocity
μ	Dynamic viscosity
ρ	Microscopic (thermodynamic) density
$\bar{\rho}$	$\alpha\rho$, the macroscopic (smear) density
σ	Surface tension
τ	Time constant

Subscripts

A	Interfacial area sources with continuous liquid
B	Interfacial area sources with continuous vapor
c	Continuous phase
Con	Saturated liquid
d	The discontinuous phase

e	E-uilibrium
g	Vapor
G	The vapor field
H	A heat-transfer source
hx	Heavier component
N	Nuclear heating
K	Frictional heating
L	Signifying liquid
Lm	A liquid energy component
ℓx	Lighter component
m	A density or energy component
m'	A density component summation index
Mix	Mixture density
P	Particles
q	A momentum component
q'	A momentum component summation index
S	The structure field
Vap	Saturated vapor
Γ	A mass-transfer source

Superscripts

I	Interface